Raman Spectroscopic Study, DFT Calculations and MD Simulations on the Conformational Isomerism of N-Alkyl-N-methylpyrrolidinium Bis-(trifluoromethanesulfonyl) Amide Ionic Liquids

ARTICLE *in* THE JOURNAL OF PHYSICAL CHEMISTRY B · MAY 2009

Impact Factor: 3.3 · DOI: 10.1021/jp9009146 · Source: PubMed

Raman Spectroscopic Study, DFT Calculations and MD Simulations on the Conformational Isomerism of *N*-Alkyl-*N*-methylpyrrolidinium Bis-(trifluoromethanesulfonyl) Amide Ionic Liquids

Yasuhiro Umebayashi,*,† Takushi Mitsugi,† Kenta Fujii,‡ Shiro Seki,§ Kazumi Chiba,|| Hideo Yamamoto,|| José N. Canongia Lopes,*,⊥ Agílio A. H. Pádua,*,# Munetaka Takeuchi,† Ryo Kanzaki,† and Shin-ichi Ishiguro†

Department of Chemistry, Faculty of Science, Kyushu University, Hakozaki, Higashi-ku, Fukuoka, 8128-8581, Japan, Materials Science Research Laboratory, Central Research Institute of Electric Power Industry (CRIEPI), 2-11-1, Iwado-kita, Komae, Tokyo 201-8511, Japan, Department of Chemistry and Applied Chemistry, Faculty of Science and Engineering, Saga University, Honjo-machi, Saga 840-8502, Japan, Japan Carlit Co. Ltd., 2470 Handa, Sibukawa-Shi, Gunma, 377-0004, Japan, Centro de Química Estrutural, Instituto Superior Técnico, 1049 001 Lisboa, and Instituto de Tecnologia Química e Biológica, UNL, Avenida República Ap. 127, 2780 901 Oeiras, Portugal, and Laboratoire Thermodynamique et Interactions Moléculaires, Université Blaise Pascal, Clermont-Ferrand/CNRS FRE3099, France

Received: January 31, 2009; Revised Manuscript Received: February 21, 2009

The conformational behaviors of *N*-alkyl-*N*-methylpyrrolidinium bis-(trifluoromethanesulfonyl) amide ionic liquids (alkyl; propyl and butyl, $[P_{1n}][TFSA]$; $n = 3$ and 4) were studied by Raman spectroscopy in the frequency range of 200−1700 cm^{-1} at different temperatures. Observed Raman spectra in the frequency range 870−960 cm^{-1} for $[P_{13}][TFSA]$ and at 860−950 cm^{-1} for $[P_{14}][TFSA]$ depend on the temperature, indicating that pseudo rotational isomerization of the pyrrolidinium ring exists in the ionic liquids. DFT calculations revealed that the pseudo rotational potential energy surfaces for P_{13}^+ and P_{14}^+ ions were similar to each other, i.e., the e6 isomer is the global minimum, whereas the three other isomers e1, e4, and e5 are ca. 3 kJ mol^{-1} higher in energy. Optimized geometries with no imaginary frequency were successfully obtained for the e6, e1, and e4 isomers. For both cations, the theoretical Raman spectra of the e6 isomers reproduce well the observed data. To explain their observed Raman spectra in a reasonable way, it is necessary to consider one or more species as predicted by DFT calculations, i.e., the e4 isomer of P_{13}^+ rather than the e1, or the e1 isomer of P_{14}^+ rather than the e4. In addition, the torsion energy potentials of the alkyl chains of the cations were scanned by DFT calculations. It turns out that the alkyl chains of the cations prefer all trans conformations. It should be emphasized that the alkyl chains of the pyrrolidinium cations show remarkably different conformational behaviors comparing with those of the imidazolium. The isomerization enthalpies $\Delta_{iso}H°$ from the e6 to the e4 isomer of P_{13}^+ and to e1 of P_{14}^+ were reasonably estimated from the temperature dependence of Raman spectra based on our proposed assignments to be 2.9 kJ mol^{-1} for P_{13}^+ and 4.2 kJ mol^{-1} for P_{14}^+, respectively. Thus evaluated experimental $\Delta_{iso}H°$ values, which may contain some uncertainties, are in agreement with those predicted by DFT calculations and MD simulations suggesting that pseudo rotational isomerization equilibria are established in the examined *N*-alkyl-*N*-methylpyrrolidinium ionic liquids. The conformational behavior of $TFSA^-$ was also investigated. The $\Delta_{iso}H°$ from the trans (trifluoromethyl groups on opposite sides of the S−N−S plane) to the cis isomer were evaluated to be 4.2 kJ mol^{-1} for $[P_{13}][TFSA]$ and 3.5 kJ mol^{-1} for $[P_{14}][TFSA]$, respectively, which are similar to that for the 1-ethyl-3methylimidazolium ionic liquid.

Introduction

Room-temperature ionic liquids have recently attracted a lot of attention as alternative solvents, because of their unique properties such as an almost null volatility and nonflammability.[1] Although many different applications in the wide and diverse field of chemistry have been found for ionic liquids in recent years, the knowledge of their fundamental physicochemical properties as liquids or solvents is still limited. One of the active research areas in ionic liquids concerns their isomerization.[2] Relatively large organic cations with a flexible alkyl chain lead to large entropy gains upon melting, and this is one of the possible reasons for the low melting point temperature of ionic liquids, though simple prediction methods based on the molar volume of ionic liquids have been proposed.[3] Recently, we have demonstrated by means of Raman spectroscopy and DFT calculations that the 1-ethyl-3-methylimidazolium (EMI^+) cation exits as part of an isomerization equilibrium in the liquid state.[4] Berg et al. have also reported the isomerization of 1-butyl-3-methylimidazolium (BMI^+) and 1-hexyl-3-methylimidazolium cations in ionic liquids.[5] High-pressure conformational behavior

* Corresponding author. E-mail: yumescc@mbox.nc.kyushu-u.ac.jp (Y.U.); jnlopes@ist.utl.pt (J.N.C.L.); and agilio.padua@univ-bpclermont.fr (A.A.H.P.).
† Kyushu University.
‡ Saga University.
§ Central Research Institute of Electric Power Industry.
|| Japan Carlit Co.
⊥ Instituto Superior Técnico.
Université Blaise Pascal.

10.1021/jp9009146 CCC: $40.75
Published on Web 03/12/2009

CHART 1: Schematic Illustrations of the *N*-Alkyl-*N*-methyl-pyrrolidinium Cation in the ax-Envelope (e1), eq-Envelope (e6), and Twist conformations, and of the Bis-(trifluoromethanesulfonyl)amide Anion, in the Gauche (C_1) and Anti (C_2) Conformations. (R = butyl and propyl)

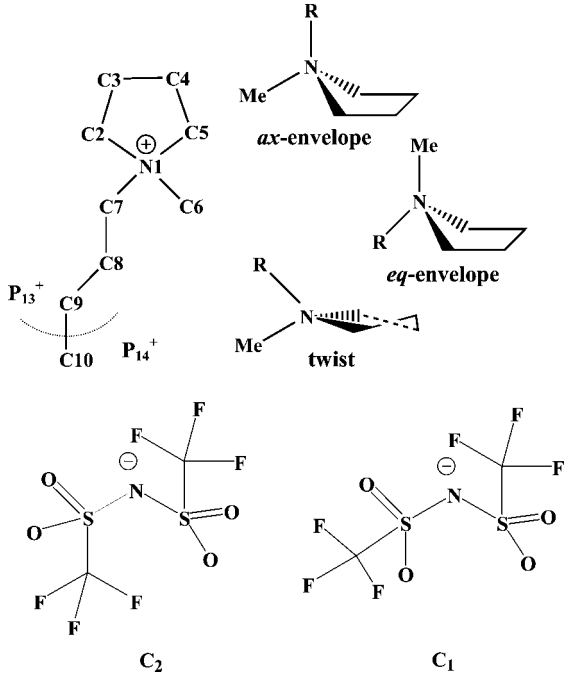

of BMI^+ was also revealed by Chang et al.[6] In addition, one of the most widely used force fields for molecular simulations of ionic liquids has been used to study their conformational behavior (in fact, the force field can yield not only structural information but also thermodynamic properties such as the density or vaporization enthalpy).[7,8] Simulations based on the above-mentioned force field satisfactorily reproduced the experimentally observed conformational behavior of 1-alkyl-3-methylimidazolium-based salts in the liquid state.[9]

The same kind of studies were also applied to large flexible anions such as bis-(trifluoromethanesulfonyl)amide ($TFSA^-$; $TFSI^-$ and Tf_2N^- are also used as the abbreviations) and bis-(fluoromethanesulfonyl)amide (FSA^-). We have so far reported the conformational isomerization equilibria of the $TFSA^-$[10] and FSA^-[11] anions combined with the EMI^+ cation. Both anions show an equilibrium between an isomer of C_2 symmetry (trans; with the CF_3 group in $TFSA^-$ and F atom in FSA^- located on opposite sides of the S−N−S planes of each ion, see Chart 1) and one of C_1 symmetry (cis), with the former at the global minimum of energy. The isomerization enthalpy of $TFSA^-$ from trans to cis was determined to be 3.5 kJ mol^{-1} in the EMI^+TFSA^- ionic liquid. A similar isomerization process of $TFSA^-$ was also observed in a nonaqueous solvent[12] and in the solid and liquid states of the tetraethylammonium salt.[13] The $TFSA^-$ isomerization in 1,3-dimethylimidazolium-based ionic liquids was elucidated by wide-angle neutron scattering experiments with empirical potential structure refinement technique, and also confirmed by MD simulations.[14] Lassègues et al. found that the solidification of [EMI][TFSA] depends on the conformations of both cation and anion, i.e., the metastable glassy solid obtained with a rapid quenching is composed mainly by the planar EMI^+ and trans $TFSA^-$ ions, whereas a slow cooling yields a crystal composed of nonplanar EMI^+ and cis $TFSA^-$ ions.[15]

CHART 2: Schematic Illustration of the pseudo Rotation of the Pyrrolidinium Ring Isomerization (R = butyl and propyl)

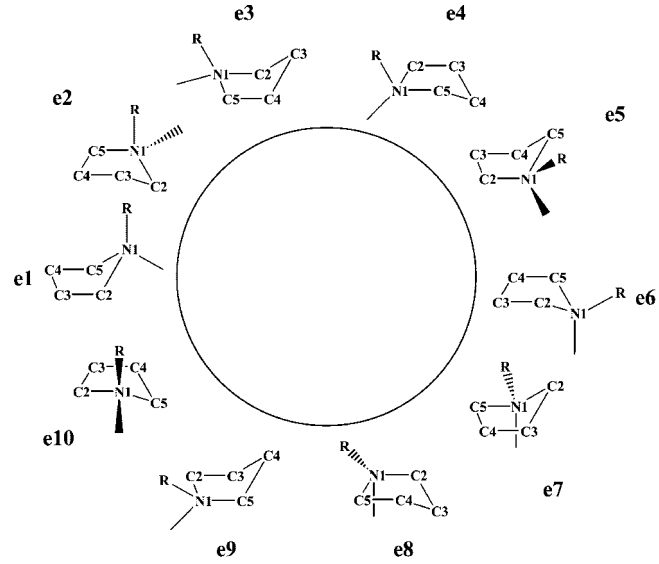

As stressed above, recent fundamental studies concerning the molecular structure or conformational behavior of ionic liquids focused mainly on compounds based on 1-alkyl-3-mehtylimidazolium cations. However, applications using ionic liquid families composed of other flexible organic cations have been recently proposed. The pyrrolidinium ion, with its aliphatic five-membered ring, exhibits 10 envelope and 10 twist conformers due to the ring pseudo rotation as shown in Chart 2. Ultrafast molecular dynamics of the pyrrolidinium ionic liquids using fentosecond optical heterodyne-detected Raman-induced Kerr effect spectroscopy (OHK-RIKES) have been reported by Shirota and Castner et al.[17] Borodin and Smith et al. have developed a many-body polarizable model for molecular simulations, and they performed MD simulations for the *N*,*N*-dimethylpyrrolidinium and *N*-methyl-*N*-propylpyrrolidinium ionic liquids based on their model.[18] In these studies, however, the isomerization of the ions in the liquid state was not discussed in detail. For a deeper understanding of the molecular and collective dynamics of ionic liquids composed of pyrrolidinium ions, it is necessary to elucidate their conformational behaviors. We have recently studied the conformational isomerism of *N*-butyl-*N*-methylpyrrolidinium (P_{14}^+) based on the pseudo rotation of the pyrrolidinium ring in the [P_{14}][TFSA] ionic liquid. In our previous study, it was proposed that the e6 isomer (eq-envelope, where the N atom is above the plane formed by the other four carbon atoms of the ring (N-envelope) and the butyl chain lies in an equatorial position relative to that plane) is at the global energy minimum, whereas the e1 isomer (ax-envelope, the other N-envelope isomer with the butyl chain in an axial position relative to the ring plane) is at a local energy minimum.[16] (Chart 1) It should be noted that the conformational isomerism of the pyrrolidinium is rather different from that of imidazolium, i.e., the latter has conformational isomerism due to the alkyl chain. However, the alkyl chain conformations of the pyrrolidinium in the ionic liquids are not so clear in our previous study.

In this paper, the conformational isomerism of *N*-alkyl-*N*-methylpyrrolidinium cations (P_{1n}^+; $n = 3$ and 4) in [P_{13}][TFSA] and [P_{14}][TFSA] ionic liquids were studied by Raman spectroscopy. We clearly demonstrate that the gauche conformers with respect to the N1−C7−C8-C9 dihedral angle of the

pyrrolidinium cations in $[P_{13}][TFSA]$ are practically negligible, which is considerably different from the imidazolium cations that have trans/gauche isomerism with respect to the corresponding dihedral angle. DFT calculations and MD simulations are also used to confirm the Raman data. The conformational behavior of the $TFSA^-$ anion present in the above-mentioned ionic liquids is also discussed. A more detailed theoretical insight into the conformational behavior of these ions, such as their potential energy landscape, has already been described elsewhere.[19]

Experimental Section

Materials. The synthesis of $[P_{14}][TFSA]$ has been previously described elsewhere.[16] A similar synthesis route has been applied to $[P_{13}][TFSA]$. The water content of the ionic liquid samples was checked by Karl Fischer, yielding less than 100 ppm. All sample preparations and treatments were performed in a glovebox of argon atmosphere with water content kept below 1.0 ppm. Density of the liquid samples was measured using a vibration tube densimeter Anton Paar DMA 5000.

Raman Spectroscopy. Raman spectra were recorded using an FT-Raman spectrometer (Perkin-Elmer GX-R) equipped with an Nd:YAG laser operating at 1064 nm. The laser power was kept at 800 mW throughout the measurements. The optical resolution was ca. 2.0 cm^{-1} and spectral data were accumulated 1024 times to achieve a good enough signal-to-noise ratio. The liquid sample in a quartz cell was stirred and thermostatted within ± 0.3 K. No detectable decomposition of the samples was found after the measurements. Recorded Raman spectra at various temperatures were normalized based on the sample liquid density and the integral intensity for the Raman band of 765 cm^{-1} ascribable to the $TFSA^-$ anion. It should be noted that this Raman band is practically independent from temperature, i.e., both isomers of C_1 and C_2 gives almost the same Raman band from our previous DFT calculations.[10]

The respective Raman spectrum at each temperature was deconvoluted to extract single Raman bands. A single Raman band is assumed to be represented as a pseudo-Voigt function, $f_V(\nu) = \gamma f_L(\nu) + (1 - \gamma) f_G(\nu)$, where $f_L(\nu)$ and $f_G(\nu)$ stand for the Lorentzian and Gaussian components, respectively, and the parameter γ $(0 < \gamma < 1)$ is the fraction of the Lorentzian component. During the curve fitting analyses, values of γ were fixed to those obtained at the lowest temperature to avoid large uncertainties arising from this parameter. In addition, the number of the model function is important, as is well-known, i.e., it may be better that the used adjustable parameters are the least in the nonlinear least-squares analyses. Therefore, we tried to reproduce the observed Raman spectra varying the number of the model function, watching the overall standard deviations and the Hamilton R factor; thus, only our final proposals were described in text. The intensity I of a single Raman band was evaluated according to $I = \gamma I_L + (1 - \gamma) I_G$, where I_L and I_G denote integrated intensities of the Lorentzian and Gaussian components, respectively. A nonlinear least-squares curve-fitting program, based on the Marquardt−Levenberg algorithm,[20,21] was developed by the authors and used throughout the analyses.

DFT Calculations. The pseudo rotational potential energy surfaces were calculated as follows; for example, with the e6 isomer, the dihedral angle C2−C3−C4−C5 in the pyrrolidinium ring was fixed to be 0°, and all of the other structural parameters were fully optimized, namely a relaxed potential energy surface, PES, was evaluated. More detailed description was given in our previous work.[22] All DFT calculations employed Becke's three-parameter hybrid method[23] with LYP correlation (B3LYP)[24] and a relatively large basis set with diffuse and polarization functions, 6−311+G(d,p), and were performed using the Gaussian03 program package[25] on the IBM eServer p5 model 595 and 570, and the Fujitsu PRIMEQUEST 580 at the Computing and Communications Center, Kyushu University.

MD Simulations. Lennard−Jones (LJ) and Coulomb terms were taken into account for intermolecular interactions. The force field constructed by Lopes and Pádua et al. was employed, which means that all simulations reported in this work are based on the OPLS-AA convention.[7] In our simulations, Gear's predictor−corrector algorithm[26] was employed for the integrals of the equation of motion. The system temperature and pressure were controlled by the Nose's[27] and the Parrinello-Rahman's[28] methods. The long-range interactions were treated by Ewald's method with the cutoff distance of 11 Å.

As the first step of the simulations, NTP ensembles at 2000 K and 10,000 atm were employed, with 256 ion pairs set at low density inside a cubic box with periodic boundary conditions. These ensembles were simulated until near-equilibrium conditions were achieved, a process that took a few hundred picoseconds. Then, the ensembles were changed to NTV, and the system volumes were fixed to the average values obtained from the previous NTP ensemble runs. These second-step equilibrations were typically calculated during 500 ps. The obtained trajectories were analyzed to check if the ions were fully mixed, and the final configurations were employed as the initial sets for the final NTP ensemble simulations at 1 atm and 298, 398, and 498 K. The final simulations typically consisted of a 1 ns equilibration period followed by 1 ns production runs. The trajectories in the last 500 ps of the production runs were then analyzed.

Density values as ensemble averages were 1.440 (5) g cm^{-3} at 298 K, 1.334 (7) g cm^{-3} at 398 K, and 1.226 (9) g cm^{-3} at 498 K for $[P_{13}][TFSA]$ and 1.393 (4), 1.292 (6), and 1.190 (9) g cm^{-3} for $[P_{14}][TFSA]$, respectively. The experimentally determined values were 1.42680 (3) and 1.39166 (2) g cm^{-3} at 298.15 K for respective ionic liquid. In addition, densities at various temperature $(293.15 < T\,(K) < 343.15)$ were measured for $[P_{13}][TFSA]$, which yields reasonable liner regression parameters against T, i.e., −0.0010783 as slope and 1.7451 as intercept, respectively. Thus experimentally estimated density values at higher temperatures are 1.316 at 398 K and 1.208 at 498 K, respectively. On the other hand, according to the IUPAC ionic liquids database, several researchers have reported experimental densities for the $[P_{13}][TFSA]$[30] and $[P_{14}][TFSA]$[31] ionic liquids. Among them, temperature dependence of the density for $[P_{14}][TFSA]$ has been explored and two sets of the linear regression parameters were published.[31a,b] The estimated values are 1.291−1.304 g cm^{-3} at 398 K and 1.186−1.213 g cm^{-3} at 498 K, respectively. In the case of both ionic liquids, the predicted densities agree with the measured or the experimentally estimated ones within ca. 1% accuracy at all temperatures examined in this work.

All simulations were carried out using Fujitsu Materials Explorer 4.0 on the Fujitsu PRIMEQUEST 580 at the Computing and Communications Center, Kyushu University.

Results and Discussion

DFT Calculations of the Pyrrolinidium Ring Pseudorotation. Figure 1 shows the pseudo rotational potential energy surfaces, PES, for the $[P_{13}]^+$ and $[P_{14}]^+$ ions. We have calculated two kinds of the pseudo rotational PES with a C6−N1−C7−C8 dihedral angle ϕ fixed to be 60 and 180° corresponding to the isomers whose alkyl chains were all trans from the ring carbon

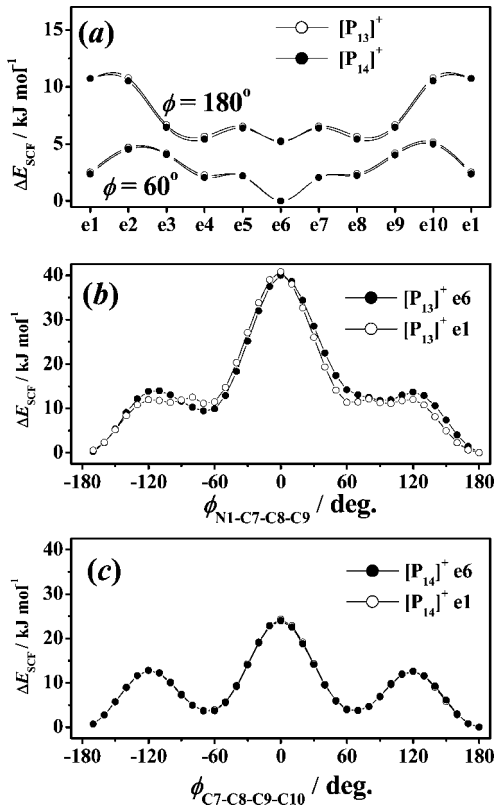

Figure 1. Potential energy curves for the pseudo rotation of the pyrrolidinium ring isomerization of (•) $[P_{14}]^+$ and (○) $[P_{13}]^+$, respectively. (a) Profiles with the C6−N1−C7−C8 dihedral angle ϕ fixed at 60 (lower curve) and 180° (upper curve), respectively, and those for the torsion with respect to (b) N1−C7−C8−C9 of $[P_{13}]^+$ and (c) C7−C8−C9−C10 of $[P_{14}]^+$, respectively. In b and c, (•) and (○) represent the pyrrolidinium ring conformations e6 and e1, respectively. All energies were calculated at the B3LYP/6−311+G(d,p) level of theory.

next to the nitrogen (C2 or C5), and from the *N*-methyl carbon (C6), respectively. As seen in Figure 1(a), when the alkyl chains are all trans from C2 or C5 carbon, the e6 isomer gives the global minimum and the other five isomers e1, e4, e5, e7, and e8 are ca. 2.5 kJ mol^{-1} higher in energy relative to the global minimum. The remaining e2, e3, e9, and e10 isomers are even more unfavorable by ca. 1.5 kJ mol^{-1}. On the other hand, the PES for the "all trans from the C6 carbon" isomer lies at even higher energies relative to the global minimum (ca. 6 kJ mol^{-1} or more), indicating that such isomers are practically negligible in terms of Raman spectroscopy.

It should be noted that there are 10 twist isomers between the corresponding 10 possible envelope isomers of each ion. Thus, it is not clear that the 10 envelope isomers are stable conformations or just saddle point geometries. Full geometry optimizations were carried out from the final geometry of each of the 10 envelope isomers obtained in the pseudo rotational PES, followed by normal-mode analyses at the optimized geometry. Fully optimized geometry was successfully obtained for the e1, e4, and e6 isomers with no imaginary frequencies (Figure 2), suggesting that these isomers are not saddle point geometries, at least as the isolated ions in gas phase are concerned. Predicted thermodynamic quantities and structural parameters for these isomers are listed in Table S1 of the Supporting Information and the normal-mode frequencies, IR intensities and Raman activities are given in Table S2 of the Supporting Information. As seen in Table S1 of the Supporting Information, the e6 isomers for both $[P_{13}]^+$ and $[P_{14}]^+$ ions are at the global minimum, and the energies corrected with zero point energy ΔE_{ZPE} for the e1 and the e4 isomers relative to the e6 are 3.7 and 3.4 kJ mol^{-1} for P_{13}^+ ion and 2.8 and 2.4 kJ mol^{-1} for P_{14}^+ ion, respectively. By taking into account the thermal energy at ambient temperature, it can be expected that the e1 and the e4 isomers coexist in equilibrium with the e6 conformer in the liquid state.

Here, it is worth comparing the alkyl chain conformation of the pyrrolodinium with that of imidazolium. We calculated the potential energy surfaces with rotating the N1−C7−C8−C9 of the $[P_{13}]^+$ and with the C7−C8−C9−C10 of the $[P_{14}]^+$. As can be seen in Figure 1b, the propyl chain of the $[P_{13}]^+$ gives two local minima of gauche isomer and global minimum of trans isomer, being practically independent from pyrolidinium ring pseudo-rotation, as expected. The gauche isomers is ca. 10 kJ mol^{-1} higher in energy relative to the trans one, suggesting that the propyl chain of the $[P_{13}]^+$ prefers trans, and the gauche isomers may be negligible in term of Raman spectroscopy. It should be remarked that the corresponding torsion potential energy surface of the imidazolium alkyl chain rather different from those of pyrrolidinium. On the other hand, in the torsion energy surface with respect to the C7−C8−C9−C10 dihedral angle, the energy difference of ca. 3.6−4.0 kJ mol^{-1} from the trans isomer to the gauche ones is relatively smaller (Figure 1c), which implies the coexistence of the gauche isomers in equilibrium with the trans one. Therefore, full geometry optimizations were carried out, and theoretical Raman spectra were also calculated at the optimized geometries with no imaginary frequency. Thus obtained theoretical Raman spectra for the gauche isomers were listed in Table S3 of the Supporting Information and were discussed in detail in the later section. ΔE_{ZPE} for the e6 isomers with the *gauche* butyl chain with respect to the C7−C8−C9−C10 dihedral angle is 4.5 and 4.3 kJ mol^{-1} for the positive and the negative dihedral angle, respectively, which is slightly larger than above-mentioned pseudo-rotational isomers such as the e1 and the e4 with a all trans butyl chain.

According to our survey of the Cambridge Structure database (CSD),[32] 7 and 12 crystals are found that contain the $[P_{13}]^+$ and $[P_{14}]^+$ ions, respectively, and among them, 15 crystallographically distinguishable structures except disordered ones are available for the respective ion. Selected structural parameters of these crystals are tabulated in Table S4 of the Supporting Information. In the crystalline solid state, e6 isomers are the most common (9 and 11) structures can be found for the $[P_{13}]^+$ and $[P_{14}]^+$ ions, respectively, which implies that, as predicted by DFT calculations, the e6 isomer is the most stable also in the crystal solid state. In the case of the $[P_{13}]^+$ ion, three e1 isomers can be found, implying that the e1 isomer has a slightly higher energy relative to the e6 isomer. At present, the e1 isomer of $[P_{14}]^+$ ion and the e4 isomers of both ions have not been found yet. In addition, with alkyl chain conformation, both [P_{13}^+] and [P_{14}^+] gauche conformers with the N1−C7−C8-C9 dihedral angle cannot be found in crystal, which well supports our conclusion deduced from Raman spectra and DFT calculations. On the other hand, we found 11 trans and 4 gauche conformers with the C7−C8−C9−C10 dihedral angle of [P_{14}^+], implying that the gauche one could be found in the liquid state.

It is also worth comparing the DFT-predicted structural parameters with those found in the crystals. We performed the comparisons with the structural parameters of the e6 isomer, for which there is a larger, more reliable, amount of data. The structural features of *N*-alkyl-*N*-methylpyrrolidinium ions predicted by DFT calculations at the B3LYP/6−311+G(d,p) level

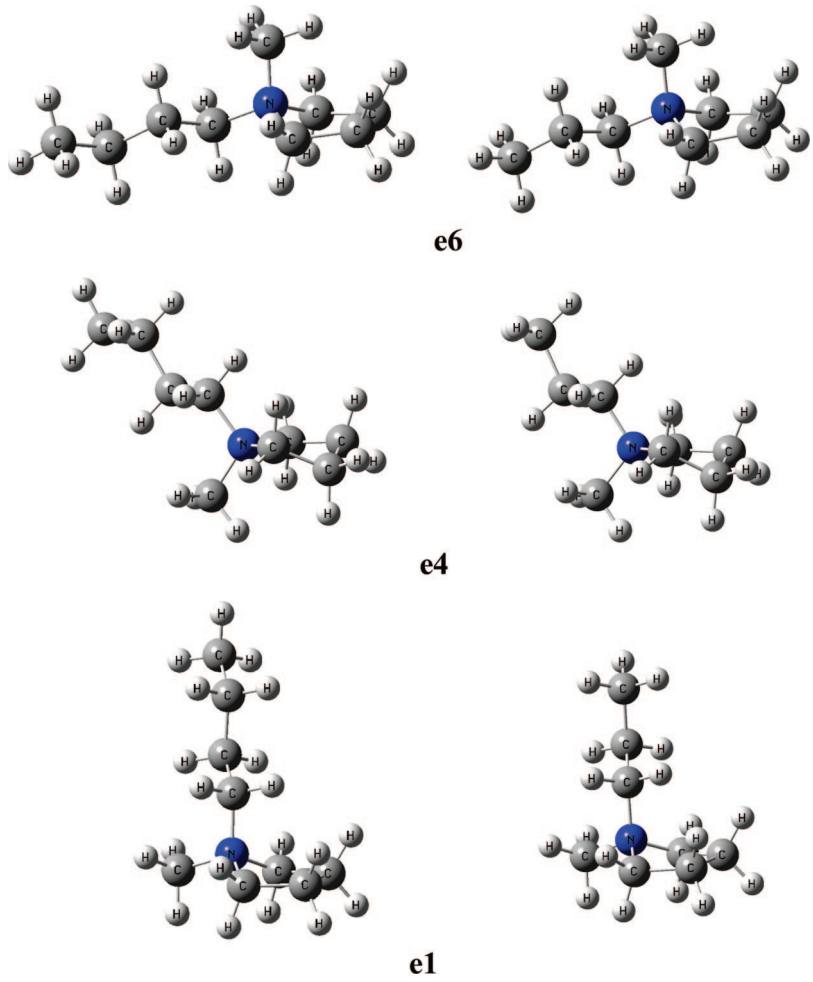

Figure 2. Optimized geometries for the e6, e4, and e1 isomers of the $[P_{14}]^+$ (left) and $[P_{13}]^+$ (right) cations, calculated at the B3LYP/6−311+G(d,p) levels of theory.

of theory are in good agreement with those found in the crystals, for instance, the C3−C4 bond length is the longest among the C−C bonds of the ion, the N1−C6 bond length is the shortest of the N1−C bonds, and the C2−N1−C5 and N1−C7−C8 angles are significantly smaller and larger, respectively, than the other angles. These similar trends can be recognized in both theoretical and experimental structural parameters of the e1 isomer. This fact indicates that the B3LYP/6−311+G(d,p) level of theory can satisfactorily predict the structural parameters of the *N*-alkyl-*N*-methylpyrrolidinium ion.

Raman Spectra and Isomerization Enthalpies. Observed Raman spectra of $[P_{13}][TFSA]$ and $[P_{14}][TFSA]$ ionic liquids at the frequency range 200−1700 cm^{-1} are shown in Figures S1 and S2 in the Supporting Information, respectively, accompanied by theoretical ones for the e1, e4, and e6 conformers of each ion. Experimental frequencies (band assignments), are also shown in Table S2 of the Supporting Information. Observed Raman spectra of $[P_{13}]^+$ agree with that previously published elsewhere.[33] With regard to both cations, most of the Raman bands observed here can be ascribable to the e6 isomers, as shown in Table S2 of the Supporting Information. The scaling factors for the e6 isomer, i.e., the slope of the linear regression of the plots of the experimental frequencies against the theoretical ones, are 0.9993 for P_{13}^+ and 1.006 for P_{14}^+, respectively. The almost identical and near-unit scaling factors indicate that the e6 isomer is the predominant conformer in both ionic liquids.

To analyze the conformational equilibrium of the pyrrolidinium ions, we measured Raman spectra for both ionic liquids

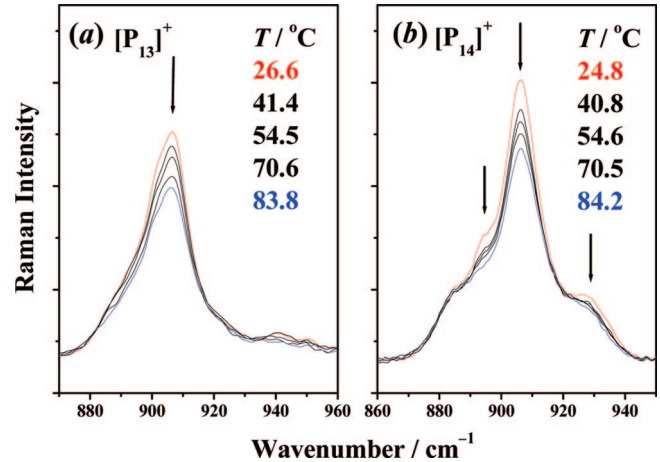

Figure 3. Temperature dependence of Raman spectra: (a) $[P_{13}][TFSA]$ in the 860−950 cm^{-1} frequency range and (b) $[P_{14}][TFSA]$ in the 870−960 cm^{-1} range.

at various temperatures. Figure 3 shows the temperature dependence of the Raman spectra at the frequency range 870−960 cm^{-1} for $[P_{13}]^+$ and 860−950 cm^{-1} for $[P_{14}]^+$, respectively. In these frequency ranges, $[TFSA]^-$ exhibits no significant Raman band. As can be seen in Figure 3, the Raman bands of $[P_{13}]^+$, at ca. 896 (shoulder), 905, and 942 cm^{-1} clearly decrease with increasing temperature, whereas that at ca. 920 cm^{-1} is practically unchanged. A similar temperature dependence was found for the $[P_{14}]^+$ ionic liquid, i.e., the Raman

bands at 892, 905, and 930 cm^{-1} obviously diminish as temperature is increased, whereas those at 883 and 917 cm^{-1} remain almost constant. This fact suggests that the equilibrium for the conformational isomerization of the pyrrolidnium ions is established in both ionic liquids. In other words, one or more conformational isomers coexist with the e6 in equilibrium.

The next step is the deconvolution of the Raman spectra, based on the theoretically calculated Raman bands, and the evaluation of the enthalpy change involved in the isomerization process. The deconvolution results are shown in Figure S3 of the Supporting Inforamtion. As indicated by DFT calculations, the energy difference between the e1 and the e4 conformers is quite small, so that it is difficult to specify one species in equilibrium with the e6 isomer among the other conformers. However, we dare to ascribe the Raman bands. With regard to $[P_{13}]^+$, the Raman spectra in the 860−950 cm^{-1} region is reproduced by assuming the existence of the e4 and the e6 isomers. The Raman bands that decrease with increasing temperature can be deconvoluted into 894, 902, 907, and 941 cm^{-1} single bands, ascribable to theoretically predicted bands at 891.7 (1.8), 898.1 (5.5), 906.1 (8.2), and 938.7 cm^{-1} (1.6) for the e6 isomers, where the values in parentheses represent the predicted Raman activities. On the other hand, the single bands at 885, 916, and 952 cm^{-1}, which are practically independent from temperature, can be assigned to theoretical bands at 889.1 (3.9), 918.1 (3.2) + 930.3 (5.7), and 945.3 cm^{-1} (1.2) for the e4 conformer, rather than the e1 one. Similarly, in the case of $[P_{14}]^+$, in order to achieve the satisfactory reproduction of the observed Raman spectra, it was necessary to take into consideration the coexistence of the e1 rather than the e4. The Raman bands that decrease with increasing temperature were fitted reasonably by the single bands at 895, 906, and 927 cm^{-1}, ascribed to the theoretical bands at 898.5 (8.1), 909.5 (10.5), and 922.4 (3.5) + 928.4 cm^{-1} (1.3) for the e6 isomer. The bands at 883 and 915 cm^{-1} were assigned to the theoretical ones at 879.1 (8.9) and 902.3 (5.8) + 912.3 cm^{-1} (8.0), respectively. It should be noted that we could not reject the existence of the e1 isomer for $[P_{13}]^+$ and the e4 for $[P_{14}]^+$. These isomers may also exist in equilibrium.

With regard to $[P_{14}]^+$, the butyl chain conformation with respect to the C7−C8−C9−C10 dihedral angle may give conformational isomers as shown in the previous section. Therefore, we attempted to compare the observed Raman spectra with those predicted by DFT calculations. As shown in Table S3 of the Supporting Information, two gauche isomers of the dihedral angle of ca. −60 and 60° have four Raman bands of 880.53 (7.1), 900.57 (14.6), 920.80 (3.5), and 931.72 cm^{-1} (1.2) for the isomer of negative dihedral angle and 884.09(8.1), 900.34 (13.8), 922.16 (2.4), and 926.74 cm^{-1} (2.2) for the other, respectively, in the corresponding frequency range. However, if we take into account the values of ΔE_{ZPE} of ca. 4.5 kJ mol^{-1} for these isomers (only 10% populations or some extent of these isomers are expected because of the value of ca. 5 kJ mol^{-1} as ΔG), it is difficult to explain the observed Raman bands of 883 cm^{-1} by considering these isomers. Moreover, we could not find the observed Raman bands ascribable to any predicted Raman bands for these isomers in the whole frequency range examined. Thus, we finally propose that the gauche isomers of the butyl chain with respect to the C7−C8−C9−C10 dihedral angle may be practically negligible in the ionic liquid of temperature range examined here.

The integral intensity, I, of a Raman band can be written as $I = Jc$, where J is the molar Raman scattering coefficient and c is the concentration of the scattering species, when the optical or apparatus coefficient is kept constant. On the other hand, if we consider that the conformational equilibrium between the X and Y isomers has an equilibrium constant K, defined as $K = [Y]/[X]$, then taking into account the relationships, $\Delta_{iso}G° = -RT\ln K$ and $\Delta_{iso}G° = \Delta_{iso}H° - T\Delta_{iso}S°$, the following relationship holds

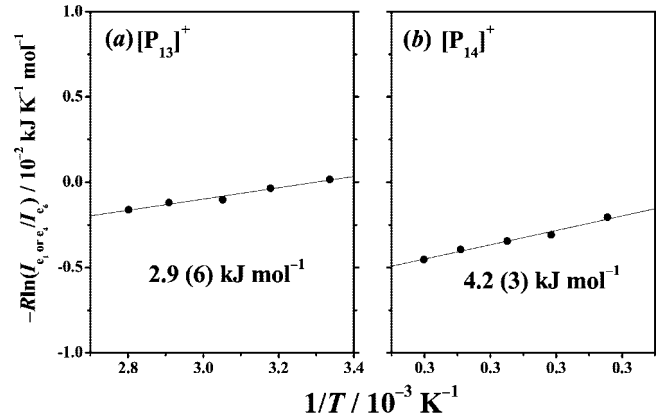

Figure 4. van't Hoff plots based on the Raman band integral intensity: (a) I_{886}/I_{906} for $[P_{13}][TFSA]$ and (b) I_{889}/I_{907} for $[P_{14}][TFSA]$.

$$-R\ln k = -R\ln([Y]/[X]) = \Delta H°(1/T) - \Delta S° \quad (1)$$

where $\Delta_{iso}G°$, $\Delta_{iso}H°$, and $\Delta_{iso}S°$ stand for the Gibbs free energy, enthalpy and entropy for the given isomerization equilibrium. The Raman integral intensity ratio can then replace the concentration ratio and be used to evaluate thermodynamic parameters from Raman spectral data, eq 2

$$R\ln(I_Y/I_X) = \Delta_{iso}H°(1/T) - \Delta_{iso}S° + R\ln(J_Y/J_X) \quad (2)$$

where the subscripts X and Y represent again the two isomeric species. This means that $\Delta_{iso}H°$ can be evaluated from the plots of the values of the left side in eq 2 against the reciprocal of temperature.

For the evaluation of $\Delta_{iso}H°$ from Raman integral intensities, we chose to analyze the pair of Raman bands at 894 and 885 cm^{-1} corresponding to the e6 and e4 isomers of $[P_{13}]^+$, respectively, and the pair at 895 and 883 cm^{-1} corresponding to the e6 and e1 isomers of $[P_{14}]^+$, respectively. These band combinations show the least superposition with other bands, among others. In fact, the analyses using these couples gave the smallest errors. The plots of $-R\ln(I_{885}/I_{894})$ for $[P_{13}]^+$ and $-RT\ln(I_{895}/I_{883})$ for $[P_{14}]^+$ against the reciprocal temperature are shown in panels a and b in Figure 4, respectively. All plots for the both ions fall on straight lines and yield values of $\Delta_{iso}H°$ of 2.9(6) kJ mol^{-1} for $[P_{13}]^+$ and 4.2(3) kJ mol^{-1} for $[P_{14}]^+$. Though the experimental evaluation of the values of $\Delta_{iso}H°$ may include some uncertainties arising from rather overlapped Raman bands, these values are in agreement with those predicted by DFT calculations, i.e., 1.6 kJ mol^{-1} and 2.4 kJ mol^{-1} for $[P_{13}]^+$ and $[P_{14}]^+$, respectively.

Figure 5 shows the temperature dependence of the Raman spectra of $[P_{13}][TFSA]$ and $[P_{14}][TFSA]$ ionic liquids at the frequency range 350−500 cm^{-1}. In both ionic liquids, the Raman band at 396 cm^{-1}, ascribable to the trans conformer of $[TFSA]^-$, decreases rather rapidly relative to the 406 cm^{-1} band of the cis isomer, when temperature is raised. Such temperature dependence is similar to that found in [EMI][TFSA] indicating that $[TFSA]^-$ isomerization hardly depends on the nature of

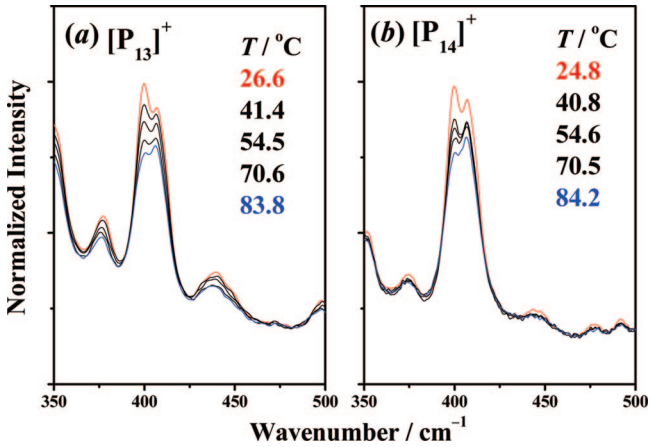

Figure 5. Temperature dependence of Raman spectra: (a) $[P_{13}][TFSA]$, and (b) $[P_{14}][TFSA]$, both in the 350−470 cm^{-1} range.

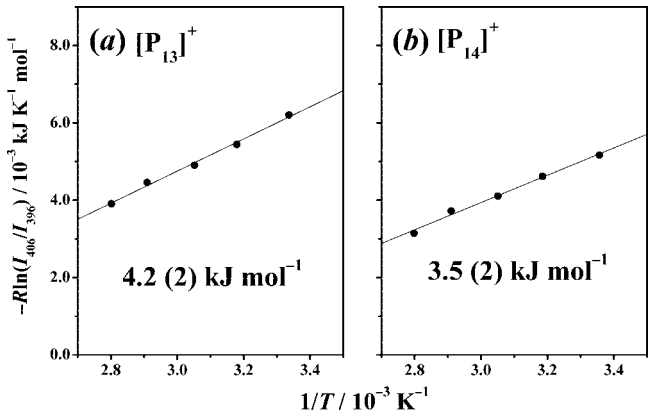

Figure 6. van't Hoff plots based on the Raman band integral intensity, I_{408}/I_{399}: (a) for $[P_{13}][TFSA]$ and (b) for $[P_{14}][TFSA]$.

the cation. Typical curve fitting results (deconvolution of the Raman spectra), based on theoretical band calculations for both cation and anion, are shown in Figure S4 in the Supporting Information. It should be noted that $[P_{13}]^+$ gives no significant Raman band at around 400 cm^{-1}. This means that the $\Delta_{iso}H°$ value determined for the $[P_{13}]^+$ ionic liquid is rather reliable. From the van't Hoff plots shown in Figure 6, $\Delta_{iso}H°$ values were successfully evaluated to be 4.2 (2) kJ mol^{-1} and 3.5 (2) kJ mol^{-1} for the isomerization of $[TFSA]^-$ in the $[P_{13}]$ [TFSA] and $[P_{14}][TFSA]$ ionic liquids, respectively. The values are in good accord with those evaluated in [EMI][TFSA] ionic liquids, which suggests that the conformational isomerization of $[TFSA]^-$ is indeed independent of the cation.

This is plausible because the interionic interaction involving such large organic cations composing the ionic liquids should not be so strong as to perturb their rotational potential energy surfaces in the liquid state. In fact, our experimental observations are in agreement with MD simulations.[9,19] Simulated CS···SC dihedral angle distributions of $TFSA^-$ in both imidazolium and pyrrolidinium ionic liquids give practically the same results.

According to our survey, 137 crystal structures containing $[TFSA]^-$ have been reported except the disordered ones, in which there are 81 and 56 anions coordinating to metal ions and nonmetal cations, respectively. Concerning the latter, the CS···SC dihedral angle distribution is shown in Figure S5a in the Supporting Information. It is clearly shown that there are two maxima in the dihedral distribution, and one can be ascribed to the trans isomer, the most probable one, and the other to the cis isomer. On the other hand, the cis $[TFSA]^-$ is preferred in the vicinity of the lithium ion both in the liquid[34] and in the crystal.[35] We have reported such preference for the cis isomer in the first solvation shell around the lithium ion in the ionic liquids by means of Raman spectra and DFT calculations.[36] The cis isomer is also preferred in the salts of alkali metals[37] and alkaline earths.[38] It is important to understand whether the $[TFSA]^-$ conformational isomerization behavior is related to the spherical shape of the metal cations or not. It should be noted that, among the crystal structures of $[TFSA]^-$ salts, dihedral distribution corresponding to those bound to metal cations are rather different from those without metal ions, as shown in Figure S5 of the Supporting Information. This suggests that specific interaction between the spherical metal ion and the anion may stabilize the cis isomer relative to the trans. Further experimental and theoretical investigation is needed on the specific interactions, and this is work in progress.

Isomerization Enthalpies Evaluated by MD Simulations. In order to discuss the *pseudo* rotational isomerization of the pyrrolidinium ring, it is worth extracting the distributions concerning the C2−C3−C4−C5 and C2−C3−N1−C7 dihedral angles. Typical dihedral angle distributions are shown in Figure S6 in the Supporting Information. As previously shown,[19] the conformational behavior of both cations are similar, which is in good agreement with DFT calculations. In the C2−C3−C4−C5 distribution, the intensity of the peak at 0° decreased with increasing temperature, while the intensity around 30° increased, suggesting that N-envelopes, the e1 and the e6 isomers, are predominant in the ionic liquids. On the other hand, typical C2−C3−N1−C7 dihedral angles are 80° for the e1 and 156° for the e6 isomers, respectively. Thus, from the C2−C3−N1−C7 dihedral angle distributions, one can find which is more stable among the isomers. Both peaks of 80 and 156° decreased with the increase in temperature. However, the latter decreased more rapidly than the former, indicating that the e6 isomer is exothermically more stable relative to the e1. Moreover, at higher temperatures, the intensity of the dihedral angle range from 90 to 150° increased, corresponding to the enhanced intensity of ca. 30° in the C2−C3−C4−C5 distribution, which suggests that the isomers not including the N-envelope one also exist, though in minority. Even if only approximately, we attempted to evaluate their isomerization enthalpies from the MD simulations. We estimated the amount of the N-envelope isomers and that of other conformers at a given temperature by using three Gaussian components in the C2−C3−C4−C5 distributions. The isomerization enthalpies thus obtained from the N-envelope conformers to the other isomers are estimated to be 7.4 kJ mol^{-1} for $[P_{13}]^+$ and 7.9 kJ mol^{-1} for $[P_{14}]^+$, respectively. Similarly, we can estimate the isomerization enthalpy from the e6 to the e1 isomer from the appropriate Gaussian fitting to the C2−C3−N1−C7 distributions. Satisfactory fitting was attained by using 5 Gaussian components, yielding isomerization enthalpies of 1.7 kJ mol^{-1} for both $[P_{13}]^+$and $[P_{14}]^+$. The values obtained from MD simulations are in good agreement with those by experimental Raman and those by DFT calculations.

It is worth comparing the conformational behavior of the alkyl chains of *N*-alkyl-*N*-methylpyrolidinium with those of the 1-alkyl-3-methylimidazolium. The distributions for the C6−N1−C7-C8 and the N1−C7−C8-C9 dihedral angles of *N*-alkyl-*N*-methylpyrrolidinium were calculated, as shown in Figure 7. In the case of the C6−N1−C7−C8 dihedral distributions, the isomers that show an trans conformation relative to the N-methyl group are much less frequent than those in the gauche conformation, as predicted by DFT calculations. For both ionic

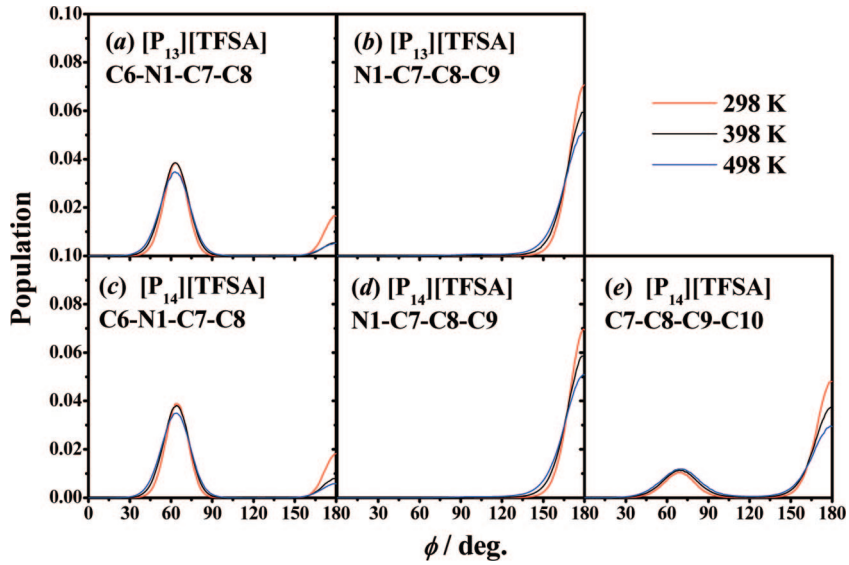

Figure 7. Dihedral angle distributions of the (a) C6−N1−C7−C8 and (b) N1−C7−C8−C9 dihedrals in $[P_{13}][TFSA]$ and the (c) C6−N1−C7−C8, (d) N1−C7−C8−C9, and (e) C7−C8−C9−C10 dihedrals in $[P_{14}][TFSA]$.

liquids, the isomerization enthalpies between the two conformers evaluated from MD simulations are 7 kJ mol^{-1}, which is also in good accordance with the energy difference predicted by DFT calculations. Looking at the N1−C7−C8−C9 dihedral distributions, we can recognize a remarkable difference from those for imidazorium ionic liquids. With both of the $[P_{13}]^+$ and the $[P_{14}]^+$ cations, the dihedral distribution gave a single peak around 180° at all temperatures examined, indicating that almost all cations in the pyrrolidinium ionic liquids show trans conformations with respect to that dihedral. On the other hand, the C7−C8−C9−C10 dihedral distribution for the $[P_{14}]^+$ cation indicates small but significant gauche isomers, with the trans isomer decreasing at higher temperatures. This implies that the gauche isomer may exist in equilibrium, though it was not so clear in the observed in Raman spectra.

Finally, we attempted to estimate the isomerizatin enthalpies from the trans to the cis isomer of the $[TFSA]^-$ anions in *N*-alkyl-*N*-methylpyrrolidinium ionic liquids from MD simulations. As shown in Figure S7, with both ionic liquids two maxima ascribable to the cis and the trans isomers were found in the CS···SC dihedral distribution, as previously reported.[19] The peak at around 165° of the trans isomer decreased more rapidly relative to the other peak at 40°, although both decreased with increasing temperature. The temperature dependence can give a clear picture at the molecular level of the phenomena underlying the Raman spectra, as previously discussed.[19] The amounts of the isomers at given temperatures were estimated as the integral intensities from 0° to 120° for the cis, and from 120 to 180° for the trans isomer, respectively. Isomerization enthalpies thus evaluated were 2.8 kJ mol^{-1} in the $[P_{13}][TFSA]$ and 2.6 kJ mol^{-1} in the $[P_{14}][TFSA]$ ionic liquids, respectively, agreeing well with those obtained by Raman and DFT calculations. Gibbs free energies of isomerization were also estimated to be ca. 0 kJ mol^{-1} for both ionic liquids.

Conclusion

Conformational behaviors of *N*-alkyl-*N*-methylpyrrolidinium bis-(trifluoromethanesulfonyl)amide ionic liquids ($[P_{13}][TFSA]$ and $[P_{14}][TFSA]$) were investigated by Raman spectroscopy. DFT calculations and MD simulations on the same systems have also been carried out. Regarding both pyrrolidinium cations, the pseudo-rotational isomerization of the 5-membered ring was recognized in the ionic liquids, i.e., two of the N-envelope isomers predominantly exist among others, and the e6 isomer of the N-envelope, with the alkyl group equatorial with respect to the C−C−C−C ring plane, can be ascribed the global minimum. The alkyl chains prefer all trans conformation starting from the carbons next to the N atom in the ring and all the way to the terminal C. Moreover, the N1−C7−C8−C9 dihedral angle distribution gives a single peak maximum of 180° for the *N*-alkyl-*N*-methylpyrrolidinium cations. Thus, the conformational behaviors of the alkyl chain in *N*-alkyl-*N*-methylpyrrolidinium ions are rather different from those in 1-alkyl-3-methylimidazolium, whose isomerization between *gauche* and *trans* occurs with in the N1−C7−C8−C9 dihedral. Isomerization of $[TFSA]^-$ from the trans to the cis isomers was also studied. The conclusions derived from both experimental Raman spectroscopy and theoretical DFT calculations and MD simulations are consistent with each other. The experimentally evaluated isomerization enthalpies in both *N*-alkyl-*N*-methylpyroolidinium ionic liquids are in good agreement with those estimated by theoretical calculations, and are similar to that evaluated in 1-alkyl-3-methylimidazolium ionic liquids.

Acknowledgment. This work has been financially supported by Grant-in-Aids for Scientific Research 19350033, 19550022, 19750062, 19003963 and 20350037.

Supporting Information Available: Figures S1−S7 and Tables S1−S3 (PDF). This material is available free of charge via the Internet at http://pubs.acs.org.

References and Notes

(1) (a) Rogers, R. D.; Seddon, K. R.; Volkov, S., Eds. *Green Industrial Applications of Ionic Liquids*; Kluwer Academic Publishers: Dordrecht, The Netherlands, 2000. (b) Rogers, R. D.; Seddon, K. R., Eds. *Ionic Liquids Industrial Applications to Green Chemistry*; ACS Symposium Series; American Chemical Society: Washington, D.C., 2002; Vol. 818. (c) Rogers, R. D.; Seddon, K. R. *Ionic liquids as Green Solvents, Progress and Properties*; ACS Symposium Series; American Chemical Society: Washington, D.C., 2003; Vol. 856. (d) Rogers, R. D.; Seddon, K. R. *Ionic liquids IIIA: Fundamentals, Progress, Challenges, and Opportunities Properties and Structure*; ACS Symposium Series; American Chemical Society: Washington, D.C., 2005; Vol. 901. (e) Rogers, R. D.; Seddon, K. R. *Ionic liquids IIIB Fundamentals, Progress, Challenges, and Opportunities*

Transformations and Processes; ACS Symposium Series; American Chemical Society: Washington, D.C., 2005; Vol. 902. (f) Ohno, H. , Ed. *Electrochemical Aspects of Ionic Liquids*; John & Wiley Sons, Inc.: Hoboken, NJ, 2005.

(2) (a) Holbrey, J. D.; Reichert, W. M.; Nieuwenhuyzen, M.; Johnston, S.; Seddon, K. R.; Rogers, R. D. *Chem. Commun.* **2003**, *163*, 6–1637. (b) Hayashi, S.; Ozawa, R.; Hamaguchi, H. *Chem. Lett.* **2003**, *32*, 498–499. (c) Saha, S.; Hayashi, S.; Kobayashi, A.; Hamaguchi, H. *Chem. Lett.* **2003**, *32*, 740–741. (d) Katayanagi, H.; Hayashi, S.; Hamaguchi, H.; Nishikawa, K. *Chem. Phys. Lett.* **2004**, *392*, 460–464.

(3) (a) Krossing, I.; Slattery, J. M.; Daguenet, C.; Dyson, P. J.; Oleinikova, A.; Weingärtner, H. *J. Am. Chem. Soc.* **2006**, *128*, 13427–13434. (b) Slattery, J. M.; Daguenet, C.; Dyson, P. J.; Schubert, T. J. S.; Krossing, I. *Angew. Chem., Int. Ed* **2007**, *46*, 5384–5388.

(4) Umebayashi, Y.; Fujimori, T.; Sukizaki, T.; Asada, M.; Fujii, K.; Kanzaki, R.; Ishiguro, S. *J. Phys. Chem. A* **2005**, *109*, 8976–8982.

(5) Berg, R. W.; Deetlefs, M.; Seddon, K. R.; Shim, I.; Thompson, J. M. *J. Phys. Chem. B* **2005**, *109*, 19018–19025.

(6) (a) Chang, H. C.; Chang, C. Y.; Su, J. C.; Chu, W. C.; Jiang, J. C.; Lin, S. H. *Int. J. Mol. Sci.* **2006**, *7*, 417–24. (b) Chang, H. C.; Jiang, J. C.; Su, J. C.; Chang, C. Y.; Lin, S. H. *J. Phys. Chem. A* **2007**, *111*, 9201–9206.

(7) (a) Lopes, J. N. C.; Deschamps, J.; Pádua, A. A. H, *J. Phys. Chem. B* **2004**, *108*, 2038–2047. (b) Lopes, J. N. C.; Pádua, A. A. H. *J. Phys. Chem. B* **2004**, *108*, 16893–16898. (c) Lopes, J. N. C.; Pádua, A. A. H. *J. Phys. Chem. B* **2006**, *110*, 19586–19592.

(8) (a) Santos, L. M. N. B. F.; Lopes, J. N. C.; Coutinho, J. A. P.; Esperança, J. M. S. S.; Gomes, L. R.; Marrucho, I. M.; Rebelo, L. P. N. *J. Am. Chem. Soc.* **2007**, *129*, 284–285. (b) Pádua, A. A. H.; Gomes, M. F. C.; Lopes, J. N. A. C. *Acc. Chem. Res.* **2007**, *40*, 1087–1096.

(9) Lopes, J. N. C.; Pádua, A. A. H. *J. Phys. Chem. B* **2006**, *110*, 7485–7489.

(10) Fujii, K.; Fujimori, T.; Takamuku, T.; Kanzaki, R.; Umebayashi, Y.; Ishiguro, S. *J. Phys. Chem. B* **2006**, *110*, 8179–8183.

(11) Fujii, K.; Seki, S.; Fukuda, S.; Kanzaki, R.; Takamuku, T.; Umebayashi, Y.; Ishiguro, S. *J. Phys. Chem. B* **2007**, *111*, 12829–12833.

(12) Herstedt, M.; Smirnov, M.; Johansson, P.; Chami, M.; Grondin, J.; Servant, L.; Lassègues, J. C. *J. Raman Spectrosc.* **2005**, *36*, 762–770.

(13) Herstedt, M.; Henderson, W. A.; Smirnov, M.; Ducasse, L.; Servant, L.; Talaga, D.; Lassègues, J. C. *J. Mol. Struct.* **2006**, *783*, 145–156.

(14) Deetlefs, M.; Hardacre, C.; Nieuwenhuyzen, M.; Padua, A. A. H.; Sheppard, O.; Soper, A. K. *J. Phys. Chem. B* **2006**, *110*, 12055–12061.

(15) Lassègues, J. C.; Grondin, J.; Holomb, R.; Johansson, P. *J. Raman Spectrosc.* **2007**, *38*, 551–558.

(16) Fujimori, T.; Fujii, K.; Kanzaki, R.; Chiba, K.; Yamamoto, H.; Umebayashi, Y.; Ishiguro, S. *J. Mol. Liq.* **2007**, *13*−*132*, 216–224.

(17) (a) Shirota, H.; Funston, A. M.; Wishart, J. F.; Castner, E. W., Jr. *J. Chem. Phys.* **2005**, *122*, 184512−1−12. (b) Castner, E. W., Jr.; Wishart, J. F.; Shirota, H. *Acc. Chem. Res.* **2007**, *40*, 1217–1227.

(18) (a) Borodin, O.; Smith, G. D. *J. Phys. Chem. B* **2006**, *110*, 11481–11490. (b) Borodin, O.; Smith, G. D.; Henderson, W. *J. Phys. Chem. B* **2006**, *110*, 16879–16886.

(19) Lopes, J. N. C.; Shimizu, K.; Pádua, A. A. H.; Umebayashi, Y.; Fukuda, S.; Fujii, K.; Ishiguro, S. *J. Phys. Chem. B* **2008**, *112*, 1465–1472.

(20) Marquardt, D. W. *J. Soc. Ind. Appl. Math.* **1963**, *11*, 431.

(21) Press, W. H.; Flannery, B. P.; Teukolsky, S. A. and Vetterling, W. T. *Numerical Recipes*; Cambridge University Press: Cambridge, U.K., 1989.

(22) Sukizaki, T.; Fukuda, S.; Yamaguchi, T.; Fujii, K.; Kanzaki, R.; Chiba, K.; Yamamoto, H.; Umebayashi, Y.; Ishiguro, S. *Electrochemisry* **2007**, *175*, 628–634.

(23) Becke, A. D. *J. Chem. Phys.* **1993**, *98*, 5648.

(24) (a) Lee, C.; Yang, W.; Parr, R. G. *Phys. Rev. B* **1988**, *37*, 785. (b) Miehlich, B.; Savin, A.; Stoll, H.; Preuss, H. *Chem. Phys. Lett.* **1989**, *157*, 200.

(25) Frisch, M. J.; Trucks, G. W.; Schlegel, H. B.; Scuseria, G. E.; Robb, M. A.; Cheeseman, J. R.; Montgomery, J. A.; Jr. , Vreven, T.; Kudin, K. N.; Burant, J. C. Millam, J. M.; Iyengar, S. S.; Tomasi, J.; Barone, V.; Mennucci, B.; Cossi, M.; Scalmani, G.; Rega, N.; Petersson, G. A.; Nakatsuji, H., Hada, M.; Ehara, M.; Toyota, K.; Fukuda, R.; Hasegawa, J.; Ishida, M.; Nakajima, T.; Honda, Y.; Kitao, O.; Nakai, H.; Klene, M.; Li, X.; Knox, J. E.; Hratchian, H. P.; Cross, J. B.; Adamo, C.; Jaramillo, J.; Gomperts, R.; Stratmann, R. E.; Yazyev, O.; Austin, A. J.; Cammi, R.; Pomelli, C.; Ochterski, J. W.; Ayala, P. Y.; Morokuma, K.; Voth, G. A.; Salvador, P.; Dannenberg, J. J.; Zakrzewski, V. G.; Dapprich, S.; Daniels, A. D.; Strain, M. C.; Farkas, O.; Malick, D. K.; Rabuck, A. D.; Raghavachari, K.; Foresman, J. B.; Ortiz, J. V.; Cui, Q.; Baboul, A. G.; Clifford, S.; Cioslowski, J.; Stefanov, B. B.; Liu, G.; Liashenko, A.; Piskorz, P.; Komaromi, I.; Martin, R. L.; Fox, D. J.; Keith, T.; Al-Laham, M. A.; Peng, C. Y.; Nanayakkara, A.; Challacombe, M.; Gill, P. M. W.; Johnson, B.; Chen, W.; Wong, M. W.; Gonzalez, C. and Pople, J. A. *Gaussian 03, Rev. B.04*; Gaussian, Inc.: Pittsburgh PA, 2003.

(26) (a) Gear, G. W. *Numerical Initial Value Problems in Ordinary Differential Equations*; Prentice Hall: Upper Saddle River, NJ, 1971. (b) Berendsen, H. J. C.; Van Gunsteren, W. F. *Proceeding of the Enrico Fermi Summer School on Molecular Dynamics Simulation of Statistical Mechanical System*; Ciccotti, G., Hover, G., Eds.; North-Holland: Amsterdam, 1986.

(27) (a) Nose, S. *Mol. Phys.* **1984**, *52*, 255. (b) Nose, S. *J. Chem. Phys.* **1984**, *81*, 511.

(28) (a) Parrinello, M.; Rahman, A. *J. Appl. Phys.* **1981**, *52*, 7182. (b) Parrinello, M.; Rahman, A. *Phys. Rev. Lett.* **1980**, *45*, 1196.

(29) *Ionic Liquids Database- (ILThermo) NIST Standard Reference Database #147*; National Institute of Standards and Technology: Gaithersburg, MD; available at http://ilthermo.boulder.nist.gov/ILThermo/mainmenu.uix.

(30) MacFarlane, D. R.; Meakin, P.; Sun, J.; Amini, N.; Forsyth, M. *J. Phys. Chem. B* **1999**, *103*, 4164–4170.

(31) (a) Anthony, J. L.; Anderson, J. L.; Maginn, E. J.; Brennecke, J. F. *J. Phys. Chem. B* **2005**, *109*, 6366–6374. (b) Kato, R.; Gmehling, J. *J. Chem. Thermodyn.* **2005**, *37*, 603–619. (c) Tokuda, H.; Tsuzuki, S.; Susan, M. A. B. H.; Hayamizu, K.; Watanabe, M. *J. Phys. Chem. B* **2006**, *110*, 19593–19600.

(32) Allen, F. H. *Acta Crystallogr., Sect. B* **2002**, *58*, 380–388.

(33) Castriota, M.; Caruso, T.; Agostino, R. G.; Cazzanelli, E.; Henderson, W. A.; Passerin, S. *J. Phys. Chem., A* **2005**, *109*, 92.

(34) Lassègues, J.; Grondin, J.; Talaga, D. *Phys. Chem. Chem. Phys.* **2006**, *8*, 5629–5632.

(35) Matsumoto, K.; Hagiwara, R.; Tamada, O. *Solid State Sci.* **2006**, *8*, 1103–1107.

(36) Umebayashi, Y.; Mitsugi, T.; Fukuda, S.; Fujimori, T.; Fujii, K.; Kanzaki, R.; Takeuchi, M.; Ishiguro, S. *J. Phys. Chem. B.* **2007**, *111*, 13028–13032.

(37) Xue, L.; Padgett, C. W.; DesMarteau, D. D.; Pennington, W. T. *Solid State Sci.* **2002**, *4*, 1535.

(38) (a) Xue, L.; DesMarteau, D. D.; Pennington, W. T. *Solid State Sci.* **2005**, *7*, 311. (b) Babai, A.; Mudring, A.-V. *Inorg. Chem.* **2006**, *45*, 3249.

JP9009146